Lagrangian postprocessing of computational hemodynamics

Shawn C. Shadden and **Amirhossein Arzani**
Mechanical Engineering, University of California, Berkeley, CA, United States

Abstract

Recent advances in imaging, modeling and computing have rapidly expanded our capabilities to model hemodynamics in the large vessels (heart, arteries and veins). This data encodes a wealth of information that is often under-utilized. Modeling (and measuring) blood flow in the large vessels typically amounts to solving for the time-varying velocity field in a region of interest. Flow in the heart and larger arteries is often complex, and velocity field data provides a starting point for investigating the hemodynamics. This data can be used to perform Lagrangian particle tracking, and other Lagrangian-based postprocessing. As described herein, Lagrangian methods are necessary to understand inherently transient hemodynamic conditions from the fluid mechanics perspective, and to properly understand the biomechanical factors that lead to acute and gradual changes of vascular function and health. The goal of the present paper is to review Lagrangian methods that have been used in post-processing velocity data of cardiovascular flows.

Keywords

advection; blood flow; coherent structures; computational fluid dynamics; modeling; particle tracking; platelets; transport

1 Introduction

The practical motivations for computational hemodynamics are to better understand blood flow in a particular region of the vasculature to (1) improve diagnosis of a cardiovascular problem, (2) better understand the hemodynamic underpinnings of cardiovascular disease initiation or progression, (3) evaluate and possibly improve how an intervention or device alters blood flow, or (4) gain more fundamental understanding of native cardiovascular function. These motivations are broad and have significant overlap.

The circulation serves to transport and exchange matter and energy throughout the body. The arteries and veins mostly serve a mechanical role in distributing blood between the heart and various microvascular beds where exchange processes take place. We restrict our discussion to the heart and larger vessels where inertial effects of blood flow are important and, in concert with local vascular morphology, can promote complex flow structures. Computational hemodynamics serves as a tool to probe such complex conditions for the

purposes described above. From the physical perspective, disturbances in blood flow influence biology in two fundamental ways, (1) by imparting *forces* on cellular elements in the vessel wall or in the blood, and (2) by enhancing or suppressing *transport* to and from various regions. Quantitative analysis of spatially resolved hemodynamics data has largely focused on determining the fluid mechanic forces imparted on the vessel wall – and namely wall shear stress for its role in endothelial function [36] and growth and remodeling [64]. Quantitative analysis of transport is less common. This is not because it is less important, but because transport is an emergent, spatiotemporal phenomenon that is difficult to quantify.

The hemodynamics in larger vessels are typically studied using computational fluid dynamics (CFD), and particularly using an image-based framework [144]. After verification and validation, an important question that arises is how to properly use, or postprocess, the resulting data. CFD can provide highly resolved spatial and temporal velocity and pressure field information. However, the purpose of computing is insight, not numbers. Image-based simulations usually deal with complex domains and pulsatile unsteady flow. From the fluid mechanics standpoint, the inherent complexity of the flow makes interpretation difficult, which is confounded by uncertainty in what about the flow is meaningful–either from the clinical, biological or even numerical perspective. Moreover, modeling or measuring fluid flow often amounts to deriving velocity data, $\mathbf{u}(\mathbf{x}, t)$. Not surprisingly, this predisposes the analysis of fluid mechanics to visualization of the velocity field, or closely related instantaneous measures. So while fluid flow, and especially blood flow, is traditionally analyzed in terms of instantaneous Eulerian fields, these measures often fail in conveying the integrated fluid behavior because their viewpoint is both frame-dependent and localized in time.

The scope of this paper is a discussion of methods used to *postprocess* hemodynamics velocity field data for purposes of understanding transport. It is biased to *Lagrangian* post-processing, which more naturally captures the spatiotemporal behavior of fluid flow than rate-of-change measures, especially when the flow topology is changing with time as is the case in most investigations of hemodynamics. The discussion mostly coincides with modeling blood as a homogeneous fluid, where blood is treated as a continuum in deriving the governing dynamics, which when solved typically provide velocity (and pressure) field information. This discussion also applies to measured velocimetry data. We do not discuss Lagrangian-based methods for modeling blood flow *dynamics* per se, e.g. methods that inherently model blood as a suspension and directly solve particle dynamics as part of the governing equations for blood flow [47]. Modeling blood as a suspension is mostly limited to very small scales and low Reynolds numbers, e.g. modeling flow in the microcirculation, where the hemodynamics are quite different than the flow in heart, arteries and veins.

2 Modeling advection from velocity data

The velocity field is the primitive variable used to describe fluid mechanics, including blood flow, and ostensibly describes how a parcel of blood, or an element carried by the blood, is transported. However, the velocity field is largely a mathematical construct, representing the *instantaneous and differential* change in a fluid element's position with time. For unsteady

flows, it is easy to misinterpret the physical behavior of the flow from inspection of the velocity data. Namely, the spatial and temporal variation of the velocity field can be simple and predictable, yet the motion of fluid elements integrated according to the velocity field alone can be surprisingly chaotic. This realization is important because it is the transport of blood elements over space and time, not the velocity field per se, that is more biologically relevant. Likewise, the relevance of other instantaneous fields derived from the velocity, or more commonly the velocity gradient (including most methods to identify "vortical" structures), to the integrated flow behavior is tenuous because a sequence of snapshots often fails to capture the *emergent* behavior of the integrated effect. Namely, it is challenging to characterize something that is always changing.

2.1 Eulerian approach

We refer to the motion of fluid elements according to the velocity field as *advection*. There are two main approaches for studying advection. The continuum approach models advection by a partial differential equation (PDE) and each fluid element is assumed to transport some property or concentration, which might not be strictly invariant due to flux on the sub-element scale (diffusion). This viewpoint commonly leads to the advection-diffusion (AD) equation modeling the transport of the scalar field $c(\mathbf{x}, t)$ according to

$$\frac{\partial c}{\partial t} + \mathbf{u} \cdot \nabla c = \nabla \cdot (\mathbf{K} \cdot \nabla c) + s, \quad (1)$$

where $\mathbf{u}(\mathbf{x}, t)$ is the velocity field that is assumed known, $\mathbf{K}$ is the diffusivity tensor, and an arbitrary source/sink (or reaction) term s has been added for generality. The material derivative on the left hand side can be thought of as an artifact of using an Eulerian viewpoint to describe the variable c. Therefore, we view the AD equation as an *Eulerian approach* to studying transport.

Non-dimensionalizing Eq. (1) using a characteristic length L, velocity magnitude u_0 and corresponding (advective) time L/u_0, along with dropping the source term and assuming isotropic diffusion ($\mathbf{K} \rightarrow \kappa$), the AD equation can be written in familiar form

$$\frac{\partial c}{\partial t} + \mathbf{u} \cdot \nabla c = \frac{1}{Pe} \nabla \cdot \nabla c, \quad (2)$$

where $Pe = u_0 L / \kappa$ is the Peclet number. For red blood cells, platelets and most macro-molecules transported in blood κ is less than $\mathcal{O}(10^{-7}$ cm^2/s) [27, 147]. For blood flow in vessels where the velocity field is typically computed or measured, $u_0 = \mathcal{O}(1-10$ cm/s) and $L = \mathcal{O}(0.1-1$ cm), yielding Peclet numbers generally larger than $\mathcal{O}(10^6)$. Recalling that Pe can be interpreted as the ratio of the diffusion response time (L^2/κ) to the advection response time (L/u_0) it is clear that transport in larger vessels is heavily advection dominated and the right hand side can often be ignored.

Eq. (2) models the evolution of a scalar field, not discrete elements or particle trajectories. Although not common, the Eulerian approach can be used to compute the trajectories of

individual fluid elements. We can "label" each material point in the domain by its initial location at some arbitrary (initial) time t_0. More formally, consider a point $(\mathbf{x}, t) \in \Omega \times I \subset \mathbb{R}^3 \times \mathbb{R}$ in space-time, which corresponds to a material point whose position as a function of time is denoted $\mathbf{x}(t)$, with $\mathbf{x}_0 \doteq \mathbf{x}(t_0)$. Then we can define a labeling $\mathbf{l} : (\mathbf{x}, t) \mapsto \mathbf{x}_0$. This labeling is unique (by uniqueness of solutions) and invariant under the flow (by definition of a material point), and thus satisfies

$$\frac{\partial \mathbf{l}}{\partial t} + \mathbf{u} \cdot \nabla \mathbf{l} = 0. \quad (3)$$

This advection equation can then be solved and individual trajectories can be obtained as the intersection of level sets $l_i(\mathbf{x}, t) = x_{0i}$ for $i = 1, 2, 3$ in extended phase space, where $\mathbf{l} = (l_1, l_2, l_3)$ and $\mathbf{x}_0 = (x_{01}, x_{02}, x_{03})$.

2.2 Lagrangian particle tracking

The alternative approach to studying advection is a (discrete) Lagrangian approach. Using this viewpoint, the position of a *material point* or *tracer* may be governed by the ordinary differential equation (ODE)

$$\dot{\mathbf{x}}(t) = \mathbf{u}(\mathbf{x}, t); \quad \mathbf{x}(t_0) = \mathbf{x}_0, \quad (4)$$

where the velocity field $\mathbf{u}(\mathbf{x}, t)$ is assumed known and $(\mathbf{x}, t) \in \Omega \times I$. Eq. (4) can be integrated to obtain the position of a tracer at a desired time

$$\mathbf{x}(t) = \mathbf{x}(t_0) + \int_{t_0}^{t} \mathbf{u}(\mathbf{x}(s), s) \, ds, \quad (5)$$

using an appropriate numerical method.

The term *Lagrangian particle tracking* is often used to describe integration of tracers. However, the term "particle" is also often used to refer to objects with non-negligible size and mass (inertial particles), as modeled using dynamic relationships (force balances) rather than the direct kinematic equation of motion above (cf. §2.3). Regardless, there are generally two main objectives in Lagrangian particle tracking. The first is to better understand the transport topology by visualization or geometric quantification of particle paths. The second is to quantify the exposure of particles to some influence as they move through the domain, such as the level of shear stress or chemical exposure experienced by a cellular or sub cellular element (e.g. platelet).

Lagrangian particle tracking has been used in several cardiovascular applications to study transport. Ehrlich and Friedman [41] performed one of the first computational particle tracking studies in blood flow using an idealized 2D bifurcation model to determine a measure of stasis as the (normalized) distance traveled by a particle over one cardiac cycle. Perktold *et al.* [110, 112, 113] studied pathlines inside idealized aneurysms and observed complicated whirling motions hypothesized to promote thrombosis. More generically, the flow inside curved vessels has been studied by constructing trajectories traced from the inlet

of the vessel to demonstrate recirculating and helical flow features [149, 56]. The carotid bifurcation is a common focus for hemodynamics research, due to the compelling correlations between atherosclerosis and separated blood flow in this region, and different studies have used particle tracking to better understand flow features in this region [111, 137, 139, 142, 92]. The effect of non-Newtonian blood rheology on tracer paths has been investigated in a 2D stenosis model [20], and in a 2D slice of an aneurysm where velocities were obtained from particle image velocimetry (PIV) [37]. Lagrangian particle tracking has also been used in evaluating surgical and device design, including optimal flow distribution in the design for the Fontan surgery [91, 157, 156]. Figure 1 shows an example of Lagrangian particle tracking for evaluating how blood is distributed in a surgery to treat congenital heart defects.

2.2.1 Comments on pathlines and trajectories—Note that solutions $\mathbf{x}(t)$ can be viewed as tracing out *curves* in Ω or in $\Omega \times I$; we refer to the former as *pathlines* and the later as *trajectories*. In this sense, a pathline is the projection of a trajectory. An implication is that pathlines of two material points may intersect each other or themselves, but trajectories do not intersect due to uniqueness of solution. We also tend to refer to the motion of a material point's position $\mathbf{x}(t)$ in Ω as its trajectory–the duality being that a trajectory can be identified as a *curve* in $\Omega \times I$, or as a *moving point* in Ω when viewed over time.

As far as visualization, it is known that for unsteady flows streamlines are of questionable utility (or even misleading) since nothing physically flows along them. Direct integration of particle trajectories is needed to better understand how material is transported through the domain. This is achieved by visualizing pathlines or viewing trajectories of particles over time, however both approaches typically provide an intertwined mess that is difficult to interpret. This is perhaps why streamlines are commonly visualized even for unsteady applications; while nothing actually flows along them, they are visually appealing since they do not intersect. While trajectories in space-time do not intersect, visualization of curves in space-time (where time is a coordinate) is unintuitive and difficult to graph.

Pathlines are often plotted to visualize the flow structure of unsteady hemodynamics data. However, the flow structure revealed is highly specific to when the pathlines are initialized – a fact that is often overlooked. The path traced out by $\mathbf{x}(t)$ depends explicitly on its location at some "initial" time. Hence, the initial position(s) and time(s) particles are seeded in the domain can play a pivotal role in what is revealed about the flow. One way to consider this is to recall pathlines as the projections of trajectories. The trajectory lives in $\Omega \times I$, and hence projecting to some hyperplane (physical 3D space), which we denote Ω_{t_0}, gives the pathlines seeded at t_0. *These projections can look completely different as the projection hyperplane Ω_{t_0} varies with t_0.* Moreover, we can have fundamentally different trajectories leading to the same pathlines.

These are not problems in steady flow, where points can be seeded and integrated forward and backward in time to map out the flow. The same is not true for pathlines for unsteady flow. Hence, pathlines in unsteady flows are inherently not as useful as pathlines (streamlines) in steady flows. As an aside, from the dynamical systems perspective, the *flow*

generated by Eq. (4) is a one-parameter family $\mathcal{F}^t : \mathbf{x}_0 \mapsto \mathbf{x}(t; \mathbf{x}_0)$ when $\mathbf{u}$ is independent of t; otherwise the flow is a two-parameter family $\mathcal{F}_{t_0}^t : \mathbf{x}_0 \mapsto \mathbf{x}(t; t_0, \mathbf{x}_0)$ for time dependent $\mathbf{u}$. One can map out the flow in space as integral curves parameterized by t for steady flows; such parameterized curves (pathlines) do not encode the flow for unsteady $\mathbf{u}$ since the extra parameter t_0 is not accommodated.

2.3 Inertial particle tracking

It is often desirable to model transport of particles in the cardiovascular system whose size and mass cannot be readily ignored. Embolic particles are an important example. Fundamental work into particle transport has a rich background in fluid mechanics, as reviewed by Michaelides [97]. The works of Maxey and Riley [95] and Gatignol [51] derive the following dynamical equation

$$
\begin{aligned}
m_p \frac{d\mathbf{v}}{dt} = & m_f \frac{D\mathbf{u}}{Dt} + (m_p - m_f)\mathbf{g} \\
& - \frac{m_f}{2} \left[\frac{d\mathbf{v}}{dt} - \frac{D}{dt} \left[\mathbf{u} - \frac{a^2}{10} \Delta \mathbf{u} \right] \right] \\
& - 6\pi a \mu \left[\mathbf{v} - \mathbf{u} - \frac{a^2}{6} \Delta \mathbf{u} \right] \\
& - \frac{6\pi a^2 \mu}{\sqrt{\pi \nu}} \int_0^t \frac{1}{\sqrt{t-\tau}} \left[\frac{d\mathbf{v}}{d\tau} - \frac{D}{Dt} \left[\mathbf{u} - \frac{a^2}{10} \Delta \mathbf{u} \right] \right] d\tau,
\end{aligned}
\tag{6}
$$

where m_p and m_f are the mass of the (spherical) particle and displaced fluid respectively; $\mathbf{g}$ is the acceleration due to gravity; $\mathbf{v}$ and $\mathbf{u}$ are the velocity of the particle and fluid; a is the particle radius; and μ and ν are the dynamic and kinematic viscosities of the fluid, and $\frac{D}{Dt}$ and $\frac{d}{dt}$ are the material derivatives following the fluid and particle. The first term on the right is the sum of the hydrodynamic forces an equivalent fluid sphere would experience. Including this term and neglecting the rest would model the particle as a fluid element, equivalent to using Eq. (4). The next term is the buoyancy force. The remaining three terms are essentially drag forces: the first is the added mass effect, the next is the steady (Stokes) drag, and the last (Boussinesq/Basset/history) term accounts for diffusion of vorticity. These last three terms include the $\mathbf{u}$ Faxen corrections, which account for local non-uniformity of the velocity field.

Equation (6) can be derived by assuming the relative Reynolds number, based on the difference between the particle velocity and the fluid velocity, is small, and that the particle is small compared to the length scale of the background flow. The application of Eq. (6) is often extended beyond these realms [97]. To a first order approximation, most emboli can be considered spherical in shape, but Eq. (6) can also be used to understand the motion of irregular particles. In such cases, the irregular particle can be modeled in terms of a equivalent diameter particle. Alternatively, if more information is known about the shape, e.g. discoid or spheroid, a theoretical or empirical correction can be added as appropriate [30, 73]. Eq. (6) does not account for hydrodynamic lift, which can be added accordingly

[96, 73] such as in locations of high shear (Saffman lift) or for rotating (Magnus lift) or non spherical particles.

An early computational study simulating inertial particle dynamics in a steady, 2D bifurcating artery was performed by Nazemi & Kleinstreue [105], and looked at impact locations of cellular (dia = 5μm sphere) particles in the bifurcation. Kleinstreuer *et al.* [65, 66, 21] later used the same methods in 3D geometries to correlate various wall shear stress (WSS) metrics to particle deposition sites. Basciano *et al.* [11] similarly looked into the transport of inertial particles inside an abdominal aortic aneurysm (AAA) with relation to stagnation and thrombus formation. These studies assumed deposition occurred when the distance of the center of the particle from the wall was within a specified threshold. Since chemical or biophysical affinity of the vessel wall and particle are likely crucial parameters for wall deposition, a more refined deposition model was proposed by Kim *et al.* [72] in the context of inertial particle tracking. Other modeling of inertial particle dynamics employed in the study of blood flow includes modeling the separation of different blood constituents [33].

Many studies including the above have primarily focused on modeling the transport of *blood cells* as inertial particles in large artery flows. This sets up inherent inconsistencies that are difficult to reconcile. Prior to applying Eq. (6), or a similar one-way coupled particle dynamics model, blood is modeled as a fluid, i.e. a continuum, to derive the velocity field **u**(**x**, *t*). In most large vessels, blood is a dense suspension, but when endowed with a proper rheology, blood can be modeled as a homogeneous fluid and the macroscopic mechanical behavior can be effectively recovered. However, this does not reasonably imply one can go back and use the flow field to model the dynamics of cellular elements as a dilute solution surrounded by a homogeneous fluid. Unlike in dilute suspensions, there is not a compelling expectation that individual cells of blood are dominated by fluid forces as described by Eq. (6). Rather intercellular collision and adhesion forces are likely as dominant, if not more dominant, than inertial and drag forces on this scale. Moreover, the fluid mechanics is not being resolved on the micron scale per se, since blood cannot be modeled as homogeneous on this scale. It is perhaps more consistent to assume cellular elements are advected by the velocity field, and possibly with diffusive (not necessarily Brownian) motion superimposed, as in e.g. [114]. That is, modeling cells as experiencing more "sub-element" effects versus "super-element" effects.

For particles whose size is large compared to that of a blood cell, blood may effectively be treated as a homogeneous fluid from the particle's perspective, which imposes hydrodynamic forces according to Eq. (6), or similar dynamical model. This may be relevant in modeling of embolic particles, which has previously been performed to model thromboemboli [107, 28]. The Stokes number (characteristic time of a particle to characteristic time of the flow) of cellular elements is typically < 0.001 in larger arteries and hence cells can be treated as material points. The Stokes number for thromboemboli can easily become close to 1. Hence an important consideration is how might the transport of inertial particles, especially to different locations in the circulation, differ from the distribution of blood flow. This is especially true for particles originating from the heart, which are a leading cause of stroke and whose possible destination is less obvious or

consequential than for particles originating elsewhere in the circulation. Carr *et al.* [28], demonstrated that the transport of inertial particles from the heart to the cerebral arteries can vary markedly from the distribution of blood flow, and the relationship to particle size is not monotonic as one might expect. Fig. 2 is a visualization of inertial particle tracking through an aortic coarctation that differentiates between particle to the upper aortic branch arteries and the descending aorta.

As consistent with the scope of this paper, Eq. 6 employs a one-way coupling whereby the particles are assumed to not affect the velocity field (and particle-particle interactions are ignored as reasonable for low particle concentrations). Whether a one way coupling is a reasonable assumption or not depends on the particular application. There are several variations in how, and to what extent, the fluid and particle dynamics may be more fully coupled. Given the complexity of cardiovascular flow modeling, few studies have investigated fully-coupled particle dynamics simulations in comparison with one-way coupling. However, in a recent study, a two-way coupling approach was used to track the distribution of particles of different size and density in circle of Willis [44], which reported a slight change in velocity contours between one- and two-way coupled methods, but did not report how that influenced particle distributions.

2.4 Lagrangian Helicity

The number of flow descriptors that have been used to characterize fluid mechanics from velocity field, or its derivatives, are too numerous to discuss. However, one descriptor that has seen repeated use in cardiovascular applications is Lagrangian helicity. Helical motion of blood flow is often observed in arteries. Helicity density is defined as the inner product of velocity $\mathbf{u}(\mathbf{x}, t)$ and vorticity $\omega(\mathbf{x}, t) = \nabla \times \mathbf{u}(\mathbf{x}, t)$ [98]. Grigioni *et al.* [56] introduced the local normalized helicity

$$\text{LNH}(\mathbf{x}, t) = \frac{\mathbf{u}(\mathbf{x}, t) \cdot \omega(\mathbf{x}, t)}{\|\mathbf{u}(\mathbf{x}, t)\| \|\omega(\mathbf{x}, t)\|}. \quad (7)$$

They integrated this measure along tracers to measure Lagrangian helicity

$$hfi_k = \frac{1}{T} \int_{t_0}^{t_0+T} |\text{LNH}_k(s)| \mathrm{d}s, \quad (8)$$

where the calculation is done for the *k*'th tracer. Repeating the calculation for different tracers a mean quantity called the helical flow index (HFI) was obtained

$$\text{HFI} = \frac{1}{N_p} \sum_{k=1}^{N_p} hfi_k \quad 0 \leq \text{HFI} \leq 1, \quad (9)$$

where N_p is the total number of tracers. Morbiducci *et al.* used this approach to quantify helicity in bypass grafts [101], aorta [103, 104], and carotid bifurcations [100, 99]. A

comparison of helical and traditional artery bypass grafts has also been done with this method [150, 162].

2.5 Simulated particle tracking for experimental data

Phase contrast (PC) magnetic resonance imaging (MRI), also referred to as PC cardiovascular magnetic resonance (CMR), is a non-invasive flow imaging technique capable of providing 3D time-resolved velocity in all three directions for large arteries in vivo. With the advances made in imaging techniques in the past years PCMRI has become an emerging tool in studying blood flow in major arteries [90, 159, 61].

The velocity field obtained by PCMRI has been commonly used for visualizing pathlines. The earliest studies have shown the feasibility of this methodology, applying it to various major arteries by forward and backward integration of velocity [23, 24]. The construction of pathlines in the aorta [16, 17, 88, 89], heart [151, 49, 18, 42, 19], heart valves [74], pulmonary artery [10], and aortic aneurysms [62, 48] has been used to visualize in vivo flow features. Figure 3 demonstrates pathlines emanating from the heart obtained from in vivo PCMRI data, created by releasing tracers in left and right ventricles.

MRI is subject to inherent measurement errors and artifacts that arise especially in complex flows. Numerical simulation of MRI has been used to understand these imaging errors. This process uses velocity data obtained from CFD to perform particle tracking of spins (magnetic moments) to reconstruct the MR image with appropriate equations. This approach has been used in studying the signal loss in magnetic resonance angiography [131], and imaging artifacts in black blood MR [138].

3 Tracking cellular damage

Thrombosis stemming from alterations in blood flow is a primary concern with nearly all major cardiovascular diseases, surgeries, and devices. Platelet activation is a critical step in the cascade of events that lead to thrombosis, and platelets can become activated chemically, or by exposure to high levels of shear (mechanical activation). Therefore, it is no surprise that velocity data from computational hemodynamics simulations has been extensively used to better understand the chemical or shear exposure of platelets as they are transported in a variety of cardiovascular flows.

Platelets are 2–4 μm in diameter. In larger artery flows, platelets have very high Peclet numbers and very small Stokes numbers, so it is reasonable to assume they are transported as material points. The exposure of platelets to pathological stresses in disturbed (high shear) flow conditions, such as through heart valves, devices and stenoses, has been of significant interest. By tracking platelets through the flow domain as discrete particles, it is common to define an activation potential (AP) as the integrated stress that the particle experiences. E.g. the activation potential defined in [127] was

$$\mathrm{AP}(\mathbf{x}_0, t_0; T) = \int_0^T \|\mathbf{e}(\mathbf{x}(t), t)\|_F \mathrm{d}t, \quad (10)$$

where **e** is the rate of strain tensor (obtained from the velocity field gradient), T is the integration length (exposure time of platelets). Alternatively, the deviatoric stress tensor σ could be used in place of **e**; the two are related by the viscosity. Some studies only incorporate "shear stress" in this definition, however experiments suggest that activation can also occur from normal stress [116]. The above AP measures both the duration that a particle remains in the domain and the level of stress that it has sustained during that time.

As noted in Sec. 2, the AP, like most Lagrangian measures, depends on the initial time and location when particles are seeded. To alleviate this problem, particles may be uniformly seeded initially, and then released at the inlet of the domain proportional to flow rate (in space and time) as to simulate a uniform density of particles continuously released and integrated through the domain, which is more or less what occurs physiologically with the seeding of platelets (ignoring the fact that platelets are thought to have higher near wall density, which may be of questionable relevance in complex flows). Regardless, since the initial location and time one starts to accumulate stress is arbitrary, one may interpret results as representing the local contribution to mechanical activation, or assuming some initial activation potential, as well as assuming only stresses above some threshold contribute to the activation potential [143].

Equation (10) quantifies the stress acting on a particle by the (Frobenius) norm of the stress tensor. Most experimental studies that have measured a stress threshold for platelet activation are based on a simple shear experiment. However, in reality all the components of the stress tensor are involved in deforming fluid elements (and potentially cellular elements). Based on Von-Mises yield criteria, setting the work done in deforming an element in a simple shear flow equal to that done by a full 3D stress tensor one obtains [3]

$$\sigma_\nu = \frac{1}{\sqrt{3}} \sqrt{\sigma_{xx}^2 + \sigma_{yy}^2 + \sigma_{zz}^2 - \sigma_{xx}\sigma_{yy} - \sigma_{xx}\sigma_{zz} - \sigma_{yy}\sigma_{zz} + 3(\sigma_{xy}^2 + \sigma_{xz}^2 + \sigma_{yz}^2)}. \quad (11)$$

Therefore, σ_ν could be used in Eq. (10) alternatively. This has been used in several computational studies to calculate AP [9, 1, 133]. It should be noted however that for incompressible flow, $\sigma_\nu = \sqrt{2}\mu \mathbf{e}_F$, and the two measures provide equivalent results. Some experimental studies have suggested that stress and exposure time should not be "weighted equally," but AP is better expressed as a power law of stress and exposure time [53, 2, 55, 106], which has been applied in several computational studies [9, 1, 102, 153, 132, 133, 12, 93].

Mechanical heart valves (MHV) have represented an important application of this type of study. Thrombosis and thromboembolism are the major complications of these devices, mainly due to mechanical platelet activation. Bluestein *et al.* [14, 13] have studied the vortex shedding phenomena behind MHVs, showing that platelets initially exposed to high shear get trapped in the formed vortices, consequently contributing to a higher AP level, similarly shown in [134]. Performance of bileaflet and monoleaflet MHVs have been compared showing higher AP levels for the bileaflet MHVs [158, 9]. The AP levels of different commercial bilieaflet MHVs has also been compared [39, 154, 160]. Different phases of

MHV closure have been studied by comparison of vorticity, shear stress, and AP [76, 54]. Morbiducci *et al.* [102] have shown that spanwise vorticity has a greater effect on platelet activation in MHVs than the streamwise vorticity. The levels of AP in bioprosthetic heart valves (BHV) have also been studied [133].

PIV is another method to obtain highly resolved velocity data to calculate AP[12], and has been compared to CFD predictions of AP giving good agreement [117]. The influence of helical flow on platelet activation has been studied in a stenosed carotid bifurcation [93]. Shadden and Hendabadi [127] have shown that AP is generally maximized near the distinguished material surfaces of the flow that control the transport mechanism (see Sec 5).

Another important application tracking cellular damage is the study of hemolysis. High levels of mechanical stress on blood cells can cause cell rupture, which leads to the release of its contents into the surrounding medium. The mechanical modeling of hemolysis is similar to platelet activation but requiring much higher levels of stress thresholds (referred to as blood damage index or hemolysis index in this context). Similar to platelet activation potential, different models have been proposed to study hemolysis taking the exposure time and stress level into account [57]. Ventricular assist devices (blood pumps) [3, 135, 136, 152, 153, 109], and MHVs [34, 132, 35, 63] have been common applications of hemolysis studies.

4 Flow Stagnation

Regions of the vasculature that are diseased or surgically-altered, and regions where vascular disease often initiates, commonly harbor flow stagnation and recirculation (e.g. aneurysms, stenosis, bifurcation zones, arterial bends, etc.). Increased residence time of atherogenic compounds, coupled with endothelial dysfunction from reduced wall shear in these locations, may be an important factor stimulating plaque formation and atherosclerosis [161]. Moreover, flow stagnation can lead to the accumulation of antagonistic compounds, platelet and blood cell aggregation, and reduced transport of natural inhibitors, leading to intravascular thrombosis. Flow stagnation is inherently a transport phenomena and hence important application of Lagrangian methods.

Particle residence time (PRT) is a common measure readily computed from particle trajectory data. A simple field definition for PRT is the minimum amount of time that a tracer with initial position $\mathbf{x}_0$ at time t_0 requires to leave a domain of interest (Γ)

$$\mathrm{PRT}(\mathbf{x}_0, t_0; \Gamma) = \min(t) \in (0, \infty) \ \text{s.t.} \ \mathbf{x}(\mathbf{x}_0, t_0 + t) \notin \Gamma, \quad (12)$$

where the tracer position $\mathbf{x}(\mathbf{x}_0, t_0 + t)$ is given by Eq. (5). The calculation of PRT requires a region Γ to be specified, which can be a subset of the computational domain. A main problem with the above definition is that it does not account for the nominal unidirectionality of blood flow, and hence locations further upstream become biased to generally higher PRT values.

Buchanan *et al.* [22] normalized PRT by the values calculated from a steady flow with the same mean Reynolds number to study the transient effects induced by changing the Womersley number in a stenosis. The effect of continuous flow from ventricular assist devices on PRT has also been evaluated [121, 115, 46]. Aneurysms are an important application of flow stagnation and recirculation. PRT in an internal carotid artery with two aneurysms has been investigated [25], as well as for abdominal aortic aneurysms (AAA). In AAA, the expansion of the aneurysm bulge together with retrograde flow induced by the renal arteries creates stagnant conditions, which have long been thought to promote aggregation of platelets and intraluminal thrombus formation (a major complication of most AAAs). Suh *et al.* [140, 141] computed PRT for several patient specific AAA demonstrating a considerable decrease in PRT during lower limb exercise due to increase in infrarenal flow rate. Arzani *et al.* [5] quantified the overall level of residence time inside different AAAs for rest and exercise conditions. Experimental techniques have also been used to evaluate PRT [69, 26, 71, 146, 45]. Figure 4 shows the procedures used for obtaining a PRT field in a AAA.

Another problem with PRT measures is that tracers that have been seeded at a particular location might get trapped later on in another location. Hence high PRT at a particular location does not necessarily reveal where stagnation/recirculation happens. To overcome this issue, the mean exposure time (MET) has been proposed [86], similar to that in [77] (termed volumetric residence time therein). MET is defined for each element or voxel *e* of the domain, and measures the accumulated amount of time that tracers entering the model spend inside this subset, as

$$\text{MET}(e) = \frac{1}{N_e \sqrt[3]{V_e}} \sum_{p=1}^{N_t} \int_0^\infty H_e(p,t)\, \mathrm{d}t$$

$$H_e = \begin{cases} 1 \text{ if } \mathbf{x}_p(t) \in e \\ 0 \text{ if } \mathbf{x}_p(t) \notin e \end{cases}, \tag{13}$$

where N_e is the number of encounters of a tracer into the element e, V_e is the volume of the element, $\mathbf{x}_p(t)$ is the position of the tracer, H_e is the indicator function of the element e, and N_t is the total number of particles released. The particle release is usually done constantly at the inlet of the domain of interest. Because of the N_e normalization, MET weighs recirculation (tracers re-entering the element) lower than stagnation (tracers staying inside the element). Similar measures without this normalization have been proposed [122]. The $\sqrt[3]{V_e}$ scaling is most reasonable for small elements, where the time spent passing through an element is proportional to length, not volume. One shortcoming of the MET measure is that it requires a high resolution of Lagrangian tracers to be released in order to sample all the computational elements sufficiently. Therefore, it is not advisable to use the flow solver elements *e*, but instead larger elements that are more commensurate with the features of interest. That is, stagnation/recirculation is something that happens over space and time and hence requires some finite-spatial scale of interest. Making elements too small renders the information rather useless–becoming effectively an inverse measure of flow speed at each location.

Gundert *et al.* computed MET for different stent designs [58]. MET has been calculated in patient specific AAAs to relate flow stagnation and progression of the aneurysm [7]. Duvernois *et al.* developed methods to perform Lagrangian postprocessing on deformable grids, demonstrating that PRT and MET calculations from deformable and rigid wall models produced similar results [40].

Longest *et al.* [83, 79] have proposed a measure to quantify near-wall residence time (NWRT) as

$$\text{NWRT} = \frac{Q_{av}}{N_t V_{NW}} \sum_{p=1}^{N_e} \int_{\text{path},p} \left(\frac{a_p}{h_p} \right)^s \frac{1}{\|\mathbf{u}_p\|} \text{d}\mathbf{r}, \quad (14)$$

where N_t is the total number of particles released, N_e is the total number of particles passing through a near wall volume (V_{NW}), Q_{av} is the average flow rate of the model used to nondimensionalize the measure, a_p is the radius of the particle, h_p is the distance between particle center and the wall, s represents an exponent set to match experimental data (set to 0 for massless particles), $\|\mathbf{u}_p\|$ is the magnitude of the particle velocity, and the integration is done along particle path (**r**). This group has used this measure to quantify stagnation in the near wall region for different applications such as grafts [83, 80, 79, 81, 82, 84], monocyte and platelet deposition [85, 78], and diseased carotid artery surgery [67]. Recently, NWRT has been used to evaluate monocyte deposition in AAAs [59].

5 Lagrangian coherent structures (LCS)

The computation of LCS seeks to overcome some important pitfalls of standard approaches to analyze flow topology. As mentioned above, characterization of unsteady flow is often performed by seeding the domain with particles and visualizing their motion. The complexity of the resulting motion and dependence on seeding strategy obscures interpretation and fundamental details of the flow. Alternatively, one can compute a scalar field of interest (residence time, helicity, vorticity, λ_2 criterion, etc.) and visualize this field. These measures can be derived from instantaneous rate of change information, or Lagrangian statistics, but in either case the field typically does little to retain/convey mechanistic understanding of transport. While in some cases the scalar field has direct clinical or biological meaning, in many cases the measure is more or less ad hoc, and interpretation depends on arbitrary color mapping or thresholding.

The reason that a simple Lagrangian tracking technique loses its capabilities in complex flows is the chaotic behavior of fluid motion. Fluid is a substance that is constantly busy getting out of its own way. However, even when viewing complex fluid motion, coherent structures can be observed. By definition, there is something "special" about these material objects, as by definition they have some persistent organizing behavior on the flow. Thus, if we restrict ourselves to viewing the fluid evolution directly, not some mathematical construct, rather than track material points at random (whose motion ends up looking random), one may seek to identify core material surfaces organizing tracer advection – which we identify as LCS.

Fluid, whether compressible or not, wants to behave as incompressible when it moves – i.e. it rather get out of its own way than bunch up. This sets up inherent saddle type hyperbolicity for fluid elements, and the elements whose direction and strength of attraction and repulsion remain most persistent are organizing features in the flow. (E.g. when "flow visualization" experiments are performed, dye is essentially used to highlight the most persistently attracting material structures.) With this viewpoint, LCS can be defined as material surfaces that are most strongly attracting or repelling – the later are hidden from dye visualization but are nonetheless important. This can be done using the right Cauchy-Green strain tensor $C(\mathbf{x}_0;t_0,t) = \nabla \mathscr{F}_{t_0}^{t}{}^{\top} \cdot \nabla \mathscr{F}_{t_0}^{t}$, where $\mathscr{F} : \mathbf{x}_0 \mapsto \mathbf{x}(t)$ is the flow map obtained e.g. from Eq. (5).

The most common method to visualize LCS is by computation of the finite time Lyapunov exponent (FTLE) field. The FTLE is essentially a scaling of the largest eigenvalue of the right Cauchy-Green strain tensor, [129] as

$$\sigma(\mathbf{x}_0;t_0,t) = \frac{1}{|t-t_0|} \ln \sqrt{\lambda_{\max} C(\mathbf{x}_0;t_0,t)}. \quad (15)$$

The natural log tends to highlight "exponential" separation and the $1/|t - t_0|$ make the measure an average growth *rate* but is mostly unnecessary in identifying LCS. FTLE measures the exponential rate of separation of nearby trajectories, a common feature of chaos. To compute the tensor field $C(\mathbf{x}_0; t_0, t)$, a grid of tracers is placed in the domain of interest and integrated forward, and the strain tensor can be computed by e.g. finite differencing nearby paths. In general, the integration length is dependent on the time scales of the flow structures. Consult [124] for a comprehensive review on FTLE/LCS calculations. *Repelling* LCS can be obtained from forward FTLE (choosing T > 0), and *attracting* LCS can be obtained from backward FTLE (T < 0). These structures have been used to extract vortex boundaries (combination of attracting and repelling LCS), flow separation (from attracting LCS) or reattachment profiles (from repelling LCS), boundaries of stagnant flow (from repelling LCS), partitions of fluid going to different downstream vessels (from repelling LCS), and mixing mechanisms (stretching and folding marked by repelling LCS and attracting LCS respectively).

These methods were first applied to cardiovascular flows in [130], who demonstrated the capabilities of this approach to track evolution of flow separation (in a carotid bifurcation), evolution of vortex boundaries (in an idealized AAA), complex mixing patterns (in a patient specific AAA), and how the partitioning of blood to downstream vessels can be mapped out (left and right pulmonary arteries in a total cavopulmonary connection). AAA represents an important application where highly complex blood flow typically occurs, which is difficult to analyze with traditional methods. Arzani and Shadden [6] used LCS to understand the detailed flow topology in several patient specific AAA showing that in all the patients the jet penetrating into the aneurysm bulge forms a vortex ring in systole, and not only the propagation of this vortex ring determines the transport topology during diastole, but also the diastole flow field dictates the fate of the penetrating vortex. An LCS capturing a large

coherent vortex in a AAA model is shown in Fig. 5. Arzani *et al.* [5] extended this analysis to study the effects of exercise and the complexities it adds to the flow topology in AAA.

The transport of blood in the left ventricle (LV) during the heart filling in diastole is another interesting application of LCS. The formation of a vortex ring inside LV enhances the optimal transport and it is correlated with ejection fraction [52]. LCS can be used as an objective method to quantify the volume of the vortex. Espa *et al.* [43] used experimental data from a heart pump to compute LCS and study the flow structures formed inside LV. LCS has also been computed from in-vivo LV PCMRI data of healthy and diseased patients [145, 29], and used to quantify the volume of the vortex ring [145]. Hendabadi *et al.* [60] computed LCS from LV Doppler-echocardiography data of healthy and diseased patients. They used attracting LCS to identify the boundaries of injection and repelling LCS as boundaries of ejection. The combination of these information was further used in their study to quantify residence time. Figure 6 contrasts characterization of flow topology using streamlines versus LCS in the LV using methods described in [60], revealing important flow structures not easily observed using traditional flow visualization.

Other studies have used this method to study transport in different aortic flows. FTLE/LCS has been computed for steady flow measured from PIV in a carotid artery showing the recirculating structures, and the increase in complexity of the structures with increase in Reynolds number [148]. LCS has been used in aortic valves to delineate the boundaries and area of the jet formed downstream of the valve [125, 8], used to quantify the severity of aortic stenosis. Xu *et al.* [155] used LCS to study blood flow during clot formation and determined regions of blood that were delivered to the clot. Duvernois *et al.* [40] computed FTLE on a deformable grid from a TCPC patient and observed little difference of the emerging LCS compared to the rigid grid. Krishnan *et al.* [75] developed a method by FTLE computations to extract vessel boundaries from PCMRI data, exploiting the fact that PCMRI gives random (noisy) velocity data for regions outside the vessel wall that lead to high FTLE values.

Schelin *et al.* [118, 120, 119] studied the chaotic advection of blood flow in idealized stenosis and aneurysm models. They used the concept of fractal dimension and Lyapunov exponents to quantify the chaotic behavior of flow. They argued that the creation of fractal structures by the chaotic flow can lead to an increase in exposure time of platelets along these structures, and the high stretching induced by these regions can enhance platelet activation. Parshar *et al.* [108] quantified chaos with Lyapunov exponents in an idealized aneurysm for different Reynolds number. Maiti *et al.* [87] looked at the effect of blood rheology corresponding to different hematocrit concentrations on the chaotic flow in a stenosis.

6 Mixing

Although LCS (Sec 5) can be effective to understand the mechanisms underlying mixing, they do not (directly) provide quantitative information on mixing or mixedness. In this section other Lagrangian approaches used to evaluate mixing are discussed. Whether mixing in cardiovascular flows is beneficial or not is not an easy question. Laminar flow in a

straight tube is unidirectional with poor mixing, however this is generally the preferred state in arteries. The situation can become more complex for diseased arteries. For example, high mixing in AAA is thought to be favorable. If there is a high global mixing in the aneurysm, platelets near the wall that are subject to aggregation and thrombosis due to stasis have a higher chance of being advected away from the wall and flushed out of the aneurysm. On the other hand, it is possible to have a region relatively cut off from the rest of the flow, but that maintains rather good mixing within itself. This is generally adverse though and can enhance thrombosis by maintaining relative stasis. Likewise, in the heart (e.g. left ventricle) an efficient momentum exchange of fluid from the inflow (mitral valve) to outflow (aortic valve) is considered beneficial, but on the other hand the heart is not emptied when it contract, and thus mixing of the residual blood volume with the injection and ejection volumes is needed. In short, secondary flow structures are beneficial for mixing, but also lead to low WSS, recirculation, pressure loss, and other undesirable characteristics.

The simplest way to evaluate mixing by Lagrangian methods is to use particle tracking and qualitatively evaluate the mixing behavior of tracers. Doorly *et al.* [38] studied the effect of vortices on mixing. They assumed that for short time intervals viscous effects can be ignored, therefore vortex lines are advected by the flow. They placed two ring of tracers aligned with the vorticity, one close to the wall and another near the axis, and tracked their evolution by particle tracking. The interaction of these two rings as they were advected by the flow was used to reveal some of the mixing features in a graft flow. The complex distribution of PRT and basins of attraction of tracers has been related to complex mixing patterns [25]. Avrahami *et al.* [9] used particle tracking to investigate the role of mixing in wash out properties of ventricular assist devices with different MHVs and the relation to thrombus formation. Combining two helical tubes with different diameters has been proposed to increase mixing in bypass grafts and arteriovenous shunts with only small pressure drops [32]. Bockman *et al.* [15] investigated the mixing of two streams of tracers from the left and right vertebral arteries into the basilar artery. Seo and Mittal [123] studied the mixing in the left ventricle by tracking tracers coming from the mitral valve, and tracers residing in the ventricle at the beginning of diastole. They sampled the domain into small volumes, and by using the standard deviation of the concentration of mitral tracers during end of diastole, and the standard deviations of unmixed, and perfect mixing conditions, they defined a mixing quality index used to quantify mixing.

Realizing that mixing is an increase in disorder of a system, the entropy concept could be used in quantification of mixing. Shannon introduced information entropy as the amount of information that a message carries (see [70])

$$S = -\sum_{x_i \in X} P(x_i) \ln \left(P(x_i) \right), \quad (16)$$

where P represents a probability measure, and the sum is over the set of all the realizations where the probability is defined on. Cookson *et al.* [31] used an alternative description of Shannon entropy and used particle tracking to quantify entropy in helical tubes such as bypass grafts. Namely,

$$S = -\sum_{i=1}^{N_c} \left(w_i \sum_{k=1}^{N_s} (n_{i,k} \log n_{i,k}) \right), \quad (17)$$

where N_c is the number of cells (used to discretize the domain), N_s is the number of species (different sets of particles whose mixing property is desired), i and k are cell and species index respectively, $n_{i,k}$ is the fraction of the k'th species in the i'th cell, and w_i is a weighting factor set to zero if the cell has no particles, or only single type particles. Equation 17 has also been used in quantifying mixing of bypass grafts with an Eulerian approach (advection-diffusion equation) [50].

The concept of Shannon entropy has been applied in dynamical systems, referred to Kolmogorov-Sinai entropy as an objective measure [68, 4]. It can be shown that under specific conditions the Kolmogorov-Sinai entropy is the spatial integral of the Lyapunov exponents of the dynamical system. In other words it measures the spectrum of all the Lyapunov exponents, and could be thought of as a measure quantifying chaotic behavior of all degrees of freedom of a system. Consequently, the close relation between chaotic transport and mixing could be observed as explained in Sec 5.

There are examples of transformations that have zero entropy but can mix specific scalar fields, furthermore the entropy measure is independent of initial configuration of the scalar field, therefore the concept of mix-norm and mix-variance has been introduced [94]. The idea is to integrate the square of the averaged values of a given scalar field over a set of subdomains (densely contained in the entire domain) to quantify mixing across all the scales. In other words, mix-norm parametrizes all the sub-domains and takes the root mean square of the average values of the scalar field across these sub-domains. Mix-variance has the same formulation but the mean of the scalar field is subtracted from the scalar field. This idea was used quantify mixing in AAAs during rest and exercise conditions in [5], by introducing two sets of tracers: fresh blood penetrating into the aneurysm, and old blood that is initially inside the aneurysm. By defining the scalar field as the concentration of fresh blood they quantified mix-norm and mix-variance and found higher and more uniform mixing during exercise. In their formulation mix-norm represents the overall percentage of fresh blood at different subdomains and mix-variance represents the overall variation in mixing at different subdomains.

7 Conclusions

Computational hemodynamics provides a powerful tool for modeling in vivo hemodynamics. Blood flow in large vessels can have fascinatingly complex behavior and understanding the nature of this complexity is one of the important challenges in hemodynamics research. Lagrangian postprocessing methods are essential in quantifying and better elucidating important features of complicated pulsatile flows. Most of these methods are based on Lagrangian particle tracking for direct visualization or geometric quantification of trajectories, or as Lagrangian framework to quantify the exposure of blood borne element as they are transported to various influences – the fluid mechanic stresses exerted on cellular elements being an important example.

While visualization of Lagrangian particle tracking alone can provide more insight into the flow topology than the velocity field or common flow characterization measures, the complex nature of trajectory data makes interoperation difficult. Quantification of broader transport behavior such as flow separation, mixing, stagnation, recirculation, etc., is often achieved by defining suitable Lagrangian-based measures that can be plotted as scalar fields. Such an approach is usually ad hoc and the scalar field of interest depends closely on the specific application, and ultimately shrouds the mechanistic behavior leading to the particular field values. LCS computation seeks a compromise by defining a scalar field from trajectory data with physical meaning, but retaining the ability to convey explicit geometric information about how fluid elements are transported.

Acknowledgments

References

1. Alemu Y, Bluestein D. Flow-induced platelet activation and damage accumulation in a mechanical heart valve: Numerical studies. Artificial Organs. 2007; 31(9):677–688. [PubMed: 17725695]

2. Anand M, Rajagopal K, Rajagopal KR. A model incorporating some of the mechanical and biochemical factors underlying clot formation and dissolution in flowing blood: Review article. Journal of Theoretical Medicine. 2003; 5(3–4):183–218.

3. Apel J, Paul R, Klaus S, Siess T, Reul H. Assessment of hemolysis related quantities in a microaxial blood pump by computational fluid dynamics. Artificial Organs. 2001; 25(5):341–347. [PubMed: 11403662]

4. Argyris, JH.; Faust, G.; Haase, M. An exploration of chaos: An introduction for natural scientists and engineers. North-Holland; Netherlands: 1994.

5. Arzani A, Les AS, Dalman RL, Shadden SC. Effect of exercise on patient specific abdominal aortic aneurysm flow topology and mixing. International Journal for Numerical Methods in Biomedical Engineering. 2014; 30(2):280–295. [PubMed: 24493404]

6. Arzani A, Shadden SC. Characterization of the transport topology in patient-specific abdominal aortic aneurysm models. Physics of Fluids. 2012; 24(8):1901.

7. Arzani, A.; Suh, GY.; McConnell, MV.; Dalman, RL.; Shadden, SC. Progression of abdominal aortic aneurysm: Effect of lagrangian transport and hemodynamic parameters. ASME 2013 Summer Bioengineering Conference; 2013; p. V01AT01A004-V01AT01A004.

8. Astorino M, Hamers J, Shadden SC, Gerbeau J. A robust and efficient valve model based on resistive immersed surfaces. International Journal for Numerical Methods in Biomedical Engineering. 2012; 28(9):937–959. [PubMed: 22941924]

9. Avrahami I, Rosenfeld M, Einav S. The hemodynamics of the berlin pul-satile VAD and the role of its MHV configuration. Annals of Biomedical Engineering. 2006; 34(9):1373–1388. [PubMed: 16838127]

10. Bächler P, Pinochet N, Sotelo J, Crelier G, Irarrazaval P, Tejos C, Uribe S. Assessment of normal flow patterns in the pulmonary circulation by using 4d magnetic resonance velocity mapping. Magnetic Resonance Imaging. 2013; 31(2):178–188. [PubMed: 22898700]

11. Basciano C, Kleinstreuer C, Hyun S, Finol EA. A relation between near-wall particle-hemodynamics and onset of thrombus formation in abdominal aortic aneurysms. Annals of Biomedical Engineering. 2011; 39(7):2010–2026. [PubMed: 21373952]

12. Bellofiore A, Quinlan NJ. High-resolution measurement of the unsteady velocity field to evaluate blood damage induced by a mechanical heart valve. Annals of Biomedical Engineering. 2011; 39(9):2417–2429. [PubMed: 21638140]

13. Bluestein D, Li YM, Krukenkamp IB. Free emboli formation in the wake of bi-leaflet mechanical heart valves and the effects of implantation techniques. Journal of Biomechanics. 2002; 35(12): 1533–1540. [PubMed: 12445606]

14. Bluestein D, Rambod E, Gharib M. Vortex shedding as a mechanism for free emboli formation in mechanical heart valves. Journal of Biomechanical Engineering. 2000; 122(2):125–134. [PubMed: 10834152]

15. Bockman MD, Kansagra AP, Shadden SC, Wong EC, Marsden AL. Fluid mechanics of mixing in the vertebrobasilar system: Comparison of simulation and MRI. Cardiovascular Engineering and Technology. 2012; 3(4):450–461.

16. Bogren HG, Buonocore MH. 4d magnetic resonance velocity mapping of blood flow patterns in the aorta in young vs. elderly normal subjects. Journal of Magnetic Resonance Imaging. 1999; 10(5):861–869. [PubMed: 10548800]

17. Hugo Bogren G, Michael Buonocore H, Richard Valente J. Four-dimensional magnetic resonance velocity mapping of blood flow patterns in the aorta in patients with atherosclerotic coronary artery disease compared to age-matched normal subjects. Journal of Magnetic Resonance Imaging. 2004; 19(4):417–427. [PubMed: 15065165]

18. Bolger AF, Heiberg E, Karlsson M, Wigström L, Engvall J, Sigfridsson A, Ebbers T, Kvitting JPE, Carlhäll CJ, Wranne B. Transit of blood flow through the human left ventricle mapped by cardiovascular magnetic resonance. Journal of Cardiovascular Magnetic Resonance. 2007; 9(5): 741–747. [PubMed: 17891610]

19. Born S, Pfeifle M, Markl M, Gutberlet M, Scheuermann G. Visual analysis of cardiac 4d MRI blood flow using line predicates. Visualization and Computer Graphics, IEEE Transactions on. 2013; 19(6):900–912.

20. Buchanan JR, Kleinstreuer C. Simulation of particle-hemodynamics in a partially occluded artery segment with implications to the initiation of microemboli and secondary stenoses. Journal of Biomechanical Engineering. 1998; 120(4):446–454. [PubMed: 10412414]

21. Buchanan JR, Kleinstreuer C, Hyun S, Truskey GA. Hemodynamics simulation and identification of susceptible sites of atherosclerotic lesion formation in a model abdominal aorta. Journal of Biomechanics. 2003; 36(8):1185–1196. [PubMed: 12831745]

22. Buchanan JR Jr, Kleinstreuer C, Comer JK. Rheological effects on pulsatile hemodynamics in a stenosed tube. Computers & Fluids. 2000; 29(6):695–724.

23. Buonocore MH. Visualizing blood flow patterns using streamlines, arrows, and particle paths. Magnetic Resonance in Medicine. 1998; 40(2):210–226. [PubMed: 9702703]

24. Buonocore MH, Bogren HG. Analysis of flow patterns using MRI. The International Journal of Cardiac Imaging. 1999; 15(2):99–103.

25. Butty VD, Gudjonsson K, Buchel P, Makhijani VB, Ventikos Y, Poulikakos D. Residence times and basins of attraction for a realistic right internal carotid artery with two aneurysms. Biorheology. 2002; 39(3):387–393. [PubMed: 12122257]

26. Cao J, Rittgers SE. Particle motion within in vitro models of stenosed internal carotid and left anterior descending coronary arteries. Annals of Biomedical Engineering. 1998; 26(2):190–199. [PubMed: 9525760]

27. Caro, CG.; Pedley, TJ.; Schroter, RC.; Seed, WA. The Mechanics of the Circulation. Oxford University Press; Oxford: 2012.

28. Carr IA, Nemoto N, Schwartz RS, Shadden SC. Size-dependent predilections of cardiogenic embolic transport. American Journal of Physiology-Heart and Circulatory Physiology. 2013; 305(5):H732–H739. [PubMed: 23792681]

29. Charonko JJ, Kumar R, Stewart K, Little WC, Vlachos PP. Vortices formed on the mitral valve tips aid normal left ventricular filling. Annals of Biomedical Engineering. 2013; 41(5):1049–1061. [PubMed: 23389556]

30. Clift, R.; Grace, JR.; Weber, ME. Bubbles, Drops, and Particles. Dover: 2005.

31. Cookson AN, Doorly DJ, Sherwin SJ. Mixing through stirring of steady flow in small amplitude helical tubes. Annals of biomedical engineering. 2009; 37(4):710–721. [PubMed: 19148753]

32. Cookson AN, Doorly DJ, Sherwin SJ. Using coordinate transformation of navier–stokes equations to solve flow in multiple helical geometries. Journal of computational and applied mathematics. 2010; 234(7):2069–2079.

33. De Gruttola S, Boomsma K, Poulikakos D. Computational simulation of a non-newtonian model of the blood separation process. Artificial Organs. 2005; 29(12):949–959. [PubMed: 16305650]

34. De Tullio MD, Cristallo A, Balaras E, Verzicco R. Direct numerical simulation of the pulsatile flow through an aortic bileaflet mechanical heart valve. Journal of Fluid Mechanics. 2009; 622:259–290.

35. De Tullio MD, Nam J, Pascazio G, Balaras E, Verzicco R. Computational prediction of mechanical hemolysis in aortic valved prostheses. European Journal of Mechanics-B/Fluids. 2012; 35:47–53.

36. DePaola N, Gimbrone MA, Davies PF, Dewey CF. Vascular endothelium responds to fluid shear stress gradients. Arteriosclerosis, Thrombosis, and Vascular Biology. 1992; 12(11):1254–7.

37. Deplano V, Knapp Y, Bailly L, Bertrand E. Flow of a blood analogue fluid in a compliant abdominal aortic aneurysm model: Experimental modelling. Journal of Biomechanics. 2014; 47(6):1262–1269. [PubMed: 24612986]

38. Doorly DJ, Sherwin SJ, Franke PT, Peiró J. Vortical flow structure identification and flow transport in arteries. Computer Methods in Biomechanics & Biomedical Engineering. 2002; 5(3): 261–273. [PubMed: 12186718]

39. Dumont K, Vierendeels J, Kaminsky R, Van Nooten G, Verdonck P, Bluestein D. Comparison of the hemodynamic and thrombogenic performance of two bileaflet mechanical heart valves using a CFD/FSI model. Journal of Biomechanical Engineering. 2007; 129(4):558–565. [PubMed: 17655477]

40. Duvernois V, Marsden AL, Shadden SC. Lagrangian analysis of hemodynamics data from FSI simulation. International Journal for Numerical Methods in Biomedical Engineering. 2013; 29(4): 445–461. [PubMed: 23559551]

41. Ehrlich LW, Friedman MH. Particle paths and stasis in unsteady flow through a bifurcation. Journal of Biomechanics. 1977; 10(9):561–568. [PubMed: 914879]

42. Eriksson J, Carlhall CJ, Dyverfeldt P, Engvall J, Bolger AF, Ebbers T. Semi-automatic quantification of 4d left ventricular blood flow. J Cardiovasc Magn Reson. 2010; 12(9):12. [PubMed: 20222980]

43. Espa S, Badas MG, Fortini S, Querzoli G, Cenedese A. A lagrangian investigation of the flow inside the left ventricle. European Journal of Mechanics-B/Fluids. 2012; 35:9–19.

44. Fabbri D, Long Q, Das S, Pinelli M. Computational modelling of emboli travel trajectories in cerebral arteries: Influence of microembolic particle size and density. Biomechanics and Modeling in Mechanobiology. 2014; 13(2):289–302. [PubMed: 24585077]

45. Falahatpisheh A, Kheradvar A. High-speed particle image velocimetry to assess cardiac fluid dynamics in vitro: From performance to validation. European Journal of Mechanics-B/Fluids. 2012; 35:2–8.

46. Filipovic N, Schima H. Numerical simulation of the flow field within the aortic arch during cardiac assist. Artificial Organs. 2011; 35(4):E73–E83. [PubMed: 21554567]

47. Freund JB. Numerical simulation of flowing blood cells. Annual Review of Fluid Mechanics. 2014; 46:67–95.

48. Frydrychowicz A, Arnold R, Hirtler D, Schlensak C, Stalder AF, Hennig J, Langer M, Markl M. Multidirectional flow analysis by cardiovascular magnetic resonance in aneurysm development following repair of aortic coarctation. Journal of Cardiovascular Magnetic Resonance. 2008; 10(1):30. [PubMed: 18538035]

49. Fyrenius A, Wigström L, Ebbers T, Karlsson M, Engvall J, Bolger AF. Three dimensional flow in the human left atrium. Heart. 2001; 86(4):448–455. [PubMed: 11559688]

50. Gambaruto AM, Moura A, Sequeira A. Topological flow structures and stir mixing for steady flow in a peripheral bypass graft with uncertainty. International Journal for Numerical Methods in Biomedical Engineering. 2010; 26(7):926–953.

51. Gatignol R. The Faxen formulae for a rigid particle in an unsteady non-uniform Stokes flow. Journal de Mecanique Theorique et Appliquee. 1983; 2(2):143–160.

52. Gharib M, Rambod E, Kheradvar A, Sahn DJ, Dabiri JO. Optimal vortex formation as an index of cardiac health. Proceedings of the National Academy of Sciences. 2006; 103(16):6305–6308.

53. Giersiepen M, Wurzinger LJ, Opitz R, Reul H. Estimation of shear stress-related blood damage in heart valve prostheses–in vitro comparison of 25 aortic valves. The International Journal of Artificial Organs. 1990; 13(5):300–306. [PubMed: 2365485]

54. Govindarajan V, Udaykumar HS, Herbertson LH, Deutsch S, Manning KB, Chandran KB. Impact of design parameters on bi-leaflet mechanical heart valve flow dynamics. The Journal of Heart Valve Disease. 2009; 18(5):535. [PubMed: 20099695]

55. Grigioni M, Daniele C, Morbiducci U, D'Avenio G, Di Benedetto G, Barbaro V. The power-law mathematical model for blood damage prediction: Analytical developments and physical inconsistencies. Artificial Organs. 2004; 28(5):467–475. [PubMed: 15113341]

56. Grigioni M, Daniele C, Morbiducci U, Del Gaudio C, D'Avenio G, Balducci A, Barbaro V. A mathematical description of blood spiral flow in vessels: Application to a numerical study of flow in arterial bending. Journal of Biomechanics. 2005; 38(7):1375–1386. [PubMed: 15922748]

57. Grigioni M, Morbiducci U, D'Avenio G, Di Benedetto G, Del Gaudio C. A novel formulation for blood trauma prediction by a modified power-law mathematical model. Biomechanics and Modeling in Mechanobiology. 2005; 4(4):249–260. [PubMed: 16283225]

58. Gundert TJ, Shadden SC, Williams AR, Koo BK, Feinstein JA, LaDisa JF Jr. A rapid and computationally inexpensive method to virtually implant current and next-generation stents into subject-specific computational fluid dynamics models. Annals of Biomedical Engineering. 2011; 39(5):1423–1437. [PubMed: 21203844]

59. Hardman D, Doyle BJ, Semple SIK, Richards JMJ, Newby DE, Easson WJ, Hoskins PR. On the prediction of monocyte deposition in abdominal aortic aneurysms using computational fluid dynamics. Proceedings of the Institution of Mechanical Engineers, Part H: Journal of Engineering in Medicine. 2013; 227(10):1114–1124.

60. Hendabadi S, Bermejo J, Benito Y, Yotti Rl, Fernández-Avilés F, del Álamo JC, Shadden SC. Topology of blood transport in the human left ventricle by novel processing of doppler echocardiography. Annals of Biomedical Engineering. 2013; 41(12):2603–2616. [PubMed: 23817765]

61. Hope MD, Wrenn SJ, Dyverfeldt P. Clinical applications of aortic 4d flow imaging. Current Cardiovascular Imaging Reports. 2013; 6(2):128–139.

62. Hope TA, Markl M, Wigström L, Alley MT, Miller DC, Herfkens RJ. Comparison of flow patterns in ascending aortic aneurysms and volunteers using four-dimensional magnetic resonance velocity mapping. Journal of Magnetic Resonance Imaging. 2007; 26(6):1471–1479. [PubMed: 17968892]

63. Hsu UK, Lu PJ. Dynamic simulation and hemolysis evaluation of the regurgitant flow over a tilting-disc mechanical heart valve in pulsatile flow. World Journal of Mechanics. 2013; 3:160.

64. Humphrey JD. Mechanisms of arterial remodeling in hypertension: coupled roles of wall shear and intramural stress. Hypertension. 2008; 52:195–200. [PubMed: 18541735]

65. Hyun S, Kleinstreuer C, Archie JP Jr. Hemodynamics analyses of arterial expansions with implications to thrombosis and restenosis. Medical Engineering & Physics. 2000; 22(1):13–27. [PubMed: 10817945]

66. Hyun S, Kleinstreuer C, Archie JP Jr. Computational particle-hemodynamics analysis and geometric reconstruction after carotid endarterectomy. Computers in Biology and Medicine. 2001; 31(5):365–384. [PubMed: 11535202]

67. Hyun S, Kleinstreuer C, Longest PW, Chen C. Particle-hemodynamics simulations and design options for surgical reconstruction of diseased carotid artery bifurcations. Journal of Biomechanical Engineering. 2004; 126(2):188–195. [PubMed: 15179848]

68. Jensen, MH.; Paladin, G.; Vulpiani, A. Dynamical systems approach to turbulence. Cambridge University Press; 2005.

69. Jin W, Clark C. Experimental investigation of unsteady flow behaviour within a sac-type ventricular assist device (VAD). Journal ofBbiomechanics. 1993; 26(6):697–707.

70. Karmeshu. Entropy measures, maximum entropy principle and emerging applications. Vol. 119. Springer; 2003.

71. Kheradvar A, Kasalko J, Johnson D, Gharib M. An in vitro study of changing profile heights in mitral bioprostheses and their influence on flow. Asaio Journal. 2006; 52(1):34–38. [PubMed: 16436888]

72. Kim MC, Nam JH, Lee CS. Near-wall deposition probability of blood elements as a new hemodynamic wall parameter. Annals of Biomedical Engineering. 2006; 34(6):958–970. [PubMed: 16783652]

73. Kleinstreuer C, Feng Y. Computational analysis of non-spherical particle transport and deposition in shear flow with application to lung aerosol dynamics—a review. Journal of Biomechanical Engineering. 2013; 135(2):021008. [PubMed: 23445053]

74. Kozerke S, Hasenkam JM, Pedersen EM, Boesiger P. Visualization of flow patterns distal to aortic valve prostheses in humans using a fast approach for cine 3d velocity mapping. Journal of Magnetic Resonance Imaging. 2001; 13(5):690–698. [PubMed: 11329190]

75. Krishnan H, Garth C, Guhring J, Gulsun MA, Greiser A, Joy KI. Analysis of time-dependent flow-sensitive PC-MRI data. Visualization and Computer Graphics, IEEE Transactions on. 2012; 18(6): 966–977.

76. Krishnan S, Udaykumar HS, Marshall JS, Chandran KB. Two-dimensional dynamic simulation of platelet activation during mechanical heart valve closure. Annals of Biomedical Engineering. 2006; 34(10):1519–1534. [PubMed: 17013660]

77. Kunov MJ, Steinman DA, Ethier CR. Particle volumetric residence time calculations in arterial geometries. Journal of Biomechanical Engineering. 1996; 118(2):158–164. [PubMed: 8738779]

78. Longest PW, Kleinstreuer C. Comparison of blood particle deposition models for non-parallel flow domains. Journal of Biomechanics. 2003; 36(3):421–430. [PubMed: 12594990]

79. Longest PW, Kleinstreuer C. Numerical simulation of wall shear stress conditions and platelet localization in realistic end-to-side arterial anastomoses. Journal of Biomechanical Engineering. 2003; 125(5):671–681. [PubMed: 14618926]

80. Longest PW, Kleinstreuer C. Particle-hemodynamics modeling of the distal end-to-side femoral bypass: Effects of graft caliber and graft-end cut. Medical Engineering & Physics. 2003; 25(10): 843–858. [PubMed: 14630472]

81. Longest PW, Kleinstreuer C, Archie JP Jr. Particle hemodynamics analysis of miller cuff arterial anastomosis. Journal of Vascular Surgery. 2003; 38(6):1353–1362. [PubMed: 14681641]

82. Longest PW, Kleinstreuer C, Buchanan JR. Efficient computation of micro-particle dynamics including wall effects. Computers & Fluids. 2004; 33(4):577–601.

83. Longest PW, Kleinstreuer C, Buchanan JR Jr. A new near-wall residence time model applied to three arterio-venous graft end-to-side anastomoses. Computer Methods in Biomechanics and Biomedical Engineering. 2001; 4(5):379–397.

84. Longest PW, Kleinstreuer C, Deanda A. Numerical simulation of wall shear stress and particle-based hemodynamic parameters in pre-cuffed and streamlined end-to-side anastomoses. Annals of Biomedical Engineering. 2005; 33(12):1752–1766. [PubMed: 16389524]

85. Longest PW, Kleinstreuer C, Truskey GA, Buchanan JR. Relation between near-wall residence times of monocytes and early lesion growth in the rabbit aorto–celiac junction. Annals of Biomedical Engineering. 2003; 31(1):53–64. [PubMed: 12572656]

86. Lonyai A, Dubin AM, Feinstein JA, Taylor CA, Shadden SC. New insights into pacemaker lead-induced venous occlusion: Simulation-based investigation of alterations in venous biomechanics. Cardiovascular Engineering. 2010; 10(2):84–90. [PubMed: 20514553]

87. Maiti S, Chaudhury K, DasGupta D, Chakraborty S. Alteration of chaotic advection in blood flow around partial blockage zone: Role of hematocrit concentration. Journal of Applied Physics. 2013; 113(3):034701.

88. Markl M, Draney MT, Hope MD, Levin JM, Chan FP, Alley MT, Pelc NJ, Herfkens RJ. Time-resolved 3-dimensional velocity mapping in the thoracic aorta: Visualization of 3-directional blood flow patterns in healthy volunteers and patients. Journal of Computer Assisted Tomography. 2004; 28(4):459–468. [PubMed: 15232376]

89. Markl M, Draney MT, Miller DC, Levin JM, Williamson EE, Pelc NJ, Liang DH, Herfkens RJ. Time-resolved three-dimensional magnetic resonance velocity mapping of aortic flow in healthy

volunteers and patients after valve-sparing aortic root replacement. The Journal of Thoracic and Cardiovascular Surgery. 2005; 130(2):456–463. [PubMed: 16077413]

90. Markl M, Kilner PJ, Ebbers T. Comprehensive 4d velocity mapping of the heart and great vessels by cardiovascular magnetic resonance. Journal of Cardiovascular Magnetic Resonance. 2011; 13(1):1–22. [PubMed: 21208447]

91. Marsden AL, Reddy VM, Shadden SC, Chan FP, Taylor CA, Feinstein JA. A new multiparameter approach to computational simulation for fontan assessment and redesign. Congenital Heart Disease. 2010; 5(2):104–117. [PubMed: 20412482]

92. Marshall I. Targeted particle tracking in computational models of human carotid bifurcations. Journal of Biomechanical Engineering. 2011; 133(12):124501. [PubMed: 22206428]

93. Massai D, Soloperto G, Gallo D, Xu XY, Morbiducci U. Shear-induced platelet activation and its relationship with blood flow topology in a numerical model of stenosed carotid bifurcation. European Journal of Mechanics-B/Fluids. 2012; 35:92–101.

94. Mathew G, Mezíc I, Petzold L. A multiscale measure for mixing. Physica D: Nonlinear Phenomena. 2005; 211(1):23–46.

95. Maxey MR, Riley JJ. Equation of motion for a small rigid sphere in a nonuniform flow. Physics of Fluids. 1983; 26(4):883–889.

96. McLaughlin JB. The lift on a small sphere in wall-bounded linear shear flows. Journal of Fluid Mechanics. 1993; 226:249–265.

97. Michaelides EE. Hydrodynamic force and heat/mass transfer from particles, bubbles, and drops—The Freeman Scholar Lecture. Journal of Fluids Engineering. 2003; 125(2):209–238.

98. Moffatt HK, Tsinober A. Helicity in laminar and turbulent flow. Annual Review of Fluid Mechanics. 1992; 24(1):281–312.

99. Morbiducci U, Gallo D, Massai D, Ponzini R, Deriu MA, Antiga L, Redaelli A, Montevecchi FM. On the importance of blood rheology for bulk flow in hemody-namic models of the carotid bifurcation. Journal of Biomechanics. 2011; 44(13):2427–2438. [PubMed: 21752380]

100. Morbiducci U, Gallo D, Ponzini R, Massai D, Antiga L, Montevecchi FM, Redaelli A. Quantitative analysis of bulk flow in image-based hemodynamic models of the carotid bifurcation: The influence of outflow conditions as test case. Annals of Biomedical Engineering. 2010; 38(12):3688–3705. [PubMed: 20589532]

101. Morbiducci U, Ponzini R, Grigioni M, Redaelli A. Helical flow as fluid dynamic signature for atherogenesis risk in aortocoronary bypass, a numeric study. Journal of Biomechanics. 2007; 40(3):519–534. [PubMed: 16626721]

102. Morbiducci U, Ponzini R, Nobili M, Massai D, Montevecchi FM, Bluestein D, Redaelli A. Blood damage safety of prosthetic heart valves, shear-induced platelet activation and local flow dynamics: A fluid–structure interaction approach. Journal of Biomechanics. 2009; 42(12):1952–1960. [PubMed: 19524927]

103. Morbiducci U, Ponzini R, Rizzo G, Cadioli M, Esposito A, De Cobelli F, Del Maschio A, Montevecchi FM, Redaelli A. In vivo quantification of helical blood flow in human aorta by time-resolved three-dimensional cine phase contrast magnetic resonance imaging. Annals of Biomedical Engineering. 2009; 37(3):516–531. [PubMed: 19142728]

104. Morbiducci U, Ponzini R, Rizzo G, Cadioli M, Esposito A, Montevecchi FM, Redaelli A. Mechanistic insight into the physiological relevance of helical blood flow in the human aorta: An in vivo study. Biomechanics and Modeling in Mechanobiology. 2011; 10(3):339–355. [PubMed: 20652615]

105. Nazemi M, Kleinstreuer C. Analysis of particle trajectories in aortic artery bifurcations with stenosis. Journal of Biomechanical Engineering. 1989; 111(4):311–315. [PubMed: 2486370]

106. Nobili J, Sheriff M, Morbiducci U, Redaelli A, Bluestein D. Platelet activation due to hemodynamic shear stresses: Damage accumulation model and comparison to in vitro measurements. ASAIO Journal (American Society for Artificial Internal Organs: 1992). 2008; 54(1):64. [PubMed: 18204318]

107. Osorio AF, Osorio R, Ceballos A, Tran R, Clark W, Divo EA, Argueta-Morales IR, Alain Kassab J, DeCampli WM. Computational fluid dynamics analysis of surgical adjustment of left

ventricular assist device implantation to minimise stroke risk. Computer Methods in Biomechanics and Biomedical Engineering. 2011; 16(6):622–638. [PubMed: 22185643]

108. Parashar A, Singh R, Panigrahi PK, Muralidhar K. Chaotic flow in an aortic aneurysm. Journal of Applied Physics. 2013; 113(21):214909.

109. Peng Y, Wu Y, Tang X, Liu W, Chen D, Gao T, Xu Y, Zeng Y. Numerical simulation and comparative analysis of flow field in axial blood pumps. Computer Methods in Biomechanics and Biomedical Engineering. 2012; 17(7):723–727. [PubMed: 22974125]

110. Perktold K. On the paths of fluid particles in an axisymmetrical aneurysm. Journal of Biomechanics. 1987; 20(3):311–317. [PubMed: 3584155]

111. Perktold K, Hilbert D. Numerical simulation of pulsatile flow in a carotid bifurcation model. Journal of Biomedical Engineering. 1986; 8(3):193–199. [PubMed: 3724122]

112. Perktold K, Kenner T, Hilbert D, Spork B, Florian H. Numerical blood flow analysis: Arterial bifurcation with a saccular aneurysm. Basic Research in Cardiology. 1988; 83(1):24–31. [PubMed: 3377740]

113. Perktold K, Peter R, Resch M. Pulsatile non-newtonian blood flow simulation through a bifurcation with an aneurysm. Biorheology. 1988; 26(6):1011–1030. [PubMed: 2624892]

114. Phillips RJ, Armstrong RC, Brown RA, Graham AL, Abbott JR. A constitutive equation for concentrated suspensions that accounts for shear-induced particle migration. Physics of Fluids A: Fluid Dynamics. 1992; 4:30–40.

115. Prosi M, Perktold K, Schima H. Effect of continuous arterial blood flow in patients with rotary cardiac assist device on the washout of a stenosis wake in the carotid bifurcation: A computer simulation study. Journal of Biomechanics. 2007; 40(10):2236–2243. [PubMed: 17157302]

116. Purvis NB Jr, Giorgio TD. The effects of elongational stress exposure on the activation and aggregation of blood platelets. Biorheology. 1991; 28(5):355. [PubMed: 1782391]

117. Raz S, Einav S, Alemu Y, Bluestein D. DPIV prediction of flow induced platelet activation–comparison to numerical predictions. Annals of Biomedical Engineering. 2007; 35(4):493–504. [PubMed: 17286206]

118. Schelin AB, Károlyi Gy, De Moura APS, Booth NA, Grebogi C. Chaotic advection in blood flow. Physical Review E. 2009; 80(1):016213.

119. Schelin AB, György Károlyi AP, De Moura S, Booth N, Grebogi C. Are the fractal skeletons the explanation for the narrowing of arteries due to cell trapping in a disturbed blood flow? Computers in Biology and Medicine. 2012; 42(3):276–281. [PubMed: 21803349]

120. Schelin AB, Károlyi György, Alessandro De Moura PS, Booth NA, Gre-bogi C. Fractal structures in stenoses and aneurysms in blood vessels. Philosophical Transactions of the Royal Society A: Mathematical, Physical and Engineering Sciences. 2010; 368(1933):5605–5617.

121. Schima H, Lackner B, Prosi M, Perktold K. Numerical simulation of carotid hemodynamics in patients with rotary blood pump cardiac assist. The International Journal of Artificial Organs. 2003; 26(2):152–160. [PubMed: 12653350]

122. Sengupta D, Kahn AM, Burns JC, Sankaran S, Shadden SC, Mars-den AL. Image-based modeling of hemodynamics in coronary artery aneurysms caused by kawasaki disease. Biomechanics and Modeling in Mechanobiology. 2012; 11(6):915–932. [PubMed: 22120599]

123. Seo JH, Mittal R. Effect of diastolic flow patterns on the function of the left ventricle. Physics of Fluids. 2013; 25(11):110801.

124. Shadden, SC. Transport and Mixing in Laminar Flows: From Microfluidics to Oceanic Currents. Wiley-VCH Verlag GmbH & Co; KGaA: 2011. Lagrangian coherent structures.

125. Shadden SC, Astorino M, Gerbeau JF. Computational analysis of an aortic valve jet with Lagrangian coherent structures. Chaos. 2010; 20:017512–1. [PubMed: 20370302]

126. Shadden SC, Dabiri JO, Marsden JE. Lagrangian analysis of fluid transport in empirical vortex rings. Physics of Fluids. 2006; 18:047105.

127. Shadden SC, Hendabadi S. Potential fluid mechanic pathways of platelet activation. Biomechanics and Modeling in Mechanobiology. 2013; 12(3):467–474. [PubMed: 22782543]

128. Shadden SC, Katija K, Rosenfeld M, Marsden JE, Dabiri JO. Transport and stirring induced by vortex formation. Journal of Fluid Mechanics. 2007; 593:315–331.

129. Shadden SC, Lekien F, Marsden JE. Definition and properties of Lagrangian coherent structures from finite-time Lyapunov exponents in two-dimensional aperiodic flows. Physica D: Nonlinear Phenomena. 2005; 212(3–4):271–304.

130. Shadden SC, Taylor CA. Characterization of coherent structures in the cardiovascular system. Annals of Biomedical Engineering. 2008; 36:1152–1162. [PubMed: 18437573]

131. Siegel JM, Oshinski JN, Pettigrew RI, Ku DN. Comparison of phantom and computer-simulated mr images of flow in a convergent geometry: Implications for improved two-dimensional MR angiography. Journal of Magnetic Resonance Imaging. 1995; 5(6):677–683. [PubMed: 8748485]

132. Simon HA, Ge L, Sotiropoulos F, Yoganathan AP. Numerical investigation of the performance of three hinge designs of bileaflet mechanical heart valves. Annals of Biomedical Engineering. 2010; 38(11):3295–3310. [PubMed: 20571852]

133. Sirois E, Sun W. Computational evaluation of platelet activation induced by a bioprosthetic heart valve. Artificial Organs. 2011; 35(2):157–165. [PubMed: 21083829]

134. Smadi O, Hassan I, Pibarot P, Kadem L. Numerical and experimental investigations of pulsatile blood flow pattern through a dysfunctional mechanical heart valve. Journal of Biomechanics. 2010; 43(8):1565–1572. [PubMed: 20188372]

135. Song X, Throckmorton AL, Wood HG, Antaki JF, Olsen DB. Computational fluid dynamics prediction of blood damage in a centrifugal pump. Artificial Organs. 2003; 27(10):938–941. [PubMed: 14616540]

136. Song X, Throckmorton AL, Wood HG, Antaki JF, Olsen DB. Quantitative evaluation of blood damage in a centrifugal VAD by computational fluid dynamics. Journal of Fluids Engineering. 2004; 126(3):410–418.

137. Steinman DA. Simulated pathline visualization of computed periodic blood flow patterns. Journal of Biomechanics. 2000; 33(5):623–628. [PubMed: 10708784]

138. Steinman DA, Rutt BK. On the nature and reduction of plaque-mimicking flow artifacts in black blood MRI of the carotid bifurcation. Magnetic Resonance in Medicine. 1998; 39(4):635–641. [PubMed: 9543426]

139. Steinman DA, Thomas JB, Ladak HM, Milner JS, Rutt BK, Spence JD. Reconstruction of carotid bifurcation hemodynamics and wall thickness using computational fluid dynamics and MRI. Magnetic Resonance in Medicine. 2002; 47(1):149–159. [PubMed: 11754454]

140. Suh GY, Les AS, Tenforde AS, Shadden SC, Spilker RL, Yeung JJ, Cheng CP, Herfkens RJ, Dalman RL, Taylor CA. Quantification of particle residence time in abdominal aortic aneurysms using magnetic resonance imaging and computational fluid dynamics. Annals of Biomedical Engineering. 2011; 39:864–883. [PubMed: 21103933]

141. Suh GY, Tenforde AS, Shadden SC, Spilker RL, Cheng CP, Herfkens RJ, Dalman RL, Taylor CA. Hemodynamic changes in abdominal aortic aneurysms with increasing exercise intensity using MR exercise imaging and image-based computational fluid dynamics. Annals of Biomedical Engineering. 2011; 39:2186–2202. [PubMed: 21509633]

142. Tambasco M, Steinman DA. On assessing the quality of particle tracking through computational fluid dynamic models. Journal of Biomechanical Engineering. 2002; 124(2):166–175. [PubMed: 12002125]

143. Tambasco M, Steinman DA. Path-dependent hemodynamics of the stenosed carotid bifurcation. Annals of Biomedical Engineering. 2003; 31(9):1054–1065. [PubMed: 14582608]

144. Taylor CA, Steinman DA. Image-based modeling of blood flow and vessel wall dynamics: Applications, methods and future directions. Annals of Biomedical Engineering. 2010; 38(3):1188–1203. [PubMed: 20087775]

145. Töger J, Kanski M, Carlsson M, Kovács SJ, Söderlind G, Arheden H, Heiberg E. Vortex ring formation in the left ventricle of the heart: Analysis by 4d flow MRI and lagrangian coherent structures. Annals of Biomedical Engineering. 2012; 40(12):2652–2662. [PubMed: 22805980]

146. Tsao R, Jones SA, Giddens DP, Zarins CK, Glagov S. An automated three-dimensional particle tracking technique for the study of modeled arterial flow fields. Journal of Biomechanical Engineering. 1995; 117(2):211–218. [PubMed: 7666658]

147. Turitto VT, Benis AM, Leonard EF. Platelet diffusion in flowing blood. Industrial and Engineering Chemistry Fundamentals. 1972; 11(2):216–223.

148. Vétel J, Garon A, Pelletier D. Lagrangian coherent structures in the human carotid artery bifurcation. Experiments in fluids. 2009; 46(6):1067–1079.

149. Wada S, Karino T. Theoretical prediction of low-density lipoproteins concentration at the luminal surface of an artery with a multiple bend. Annals of Biomedical Engineering. 2002; 30(6):778–791. [PubMed: 12220078]

150. Wen J, Zheng T, Jiang W, Deng X, Fan Y. A comparative study of helical-type and traditional-type artery bypass grafts: Numerical simulation. ASAIO Journal. 2011; 57(5):399–406. [PubMed: 21869617]

151. Wigström L, Ebbers T, Fyrenius A, Karlsson M, Engvall J, Wranne B, Bolger AF. Particle trace visualization of intracardiac flow using time-resolved 3d phase contrast MRI. Magnetic Resonance in Medicine. 1999; 41(4):793–799. [PubMed: 10332856]

152. Wu J, Antaki JF, Snyder TA, Wagner WR, Borovetz HS, Paden BE. Design optimization of blood shearing instrument by computational fluid dynamics. Artificial Organs. 2005; 29(6):482–489. [PubMed: 15926986]

153. Wu J, Paden BE, Borovetz HS, Antaki JF. Computational fluid dynamics analysis of blade tip clearances on hemodynamic performance and blood damage in a centrifugal ventricular assist device. Artificial Organs. 2010; 34(5):402–411. [PubMed: 19832736]

154. Xenos M, Girdhar G, Alemu Y, Jesty J, Slepian M, Einav S, Bluestein D. Device thrombogenicity emulator (DTE)-design optimization methodology for cardiovascular devices: A study in two bileaflet MHV designs. Journal of Biomechanics. 2010; 43(12):2400–2409. [PubMed: 20483411]

155. Xu Z, Chen N, Shadden SC, Marsden JE, Kamocka MM, Rosen ED, Alber M. Study of blood flow impact on growth of thrombi using a multiscale model. Soft Matter. 2009; 5(4):769–779.

156. Yang W, Feinstein JA, Shadden SC, Vignon-Clementel IE, Marsden AL. Optimization of a Y-graft design for improved hepatic flow distribution in the Fontan circulation. Journal of Biomechanical Engineering. 2013; 135(1):011002. [PubMed: 23363213]

157. Yang W, Vignon-Clementel IE, Troianowski G, Reddy VM, Feinstein JA, Marsden AL. Hepatic blood flow distribution and performance in conventional and novel Y-graft Fontan geometries: A case series computational fluid dynamics study. The Journal of Thoracic and Cardiovascular Surgery. 2012; 143(5):1086–1097. [PubMed: 21962841]

158. Yin W, Alemu Y, Affeld K, Jesty J, Bluestein D. Flow-induced platelet activation in bileaflet and monoleaflet mechanical heart valves. Annals of Biomedical Engineering. 2004; 32(8):1058–1066. [PubMed: 15446502]

159. Young AA, Prince JL. Cardiovascular magnetic resonance: Deeper insights through bioengineering. Annual Review of Biomedical Engineering. 2013; 15:433–461.

160. Yun BM, Wu J, Simon HA, Arjunon S, Sotiropoulos F, Aidun CK, Yoganathan AP. A numerical investigation of blood damage in the hinge area of aortic bileaflet mechanical heart valves during the leakage phase. Annals of Biomedical Engineering. 2012; 40(7):1468–1485. [PubMed: 22215278]

161. Zarins, CK.; Glagov, S. Vascular Surgery Principles and Practice, chapter Pathophysiology of human atherosclerosis. McGraw-Hill; 1994.

162. Zheng T, Wang W, Jiang W, Deng X, Fan Y. Assessing hemodynamic performances of small diameter helical grafts: Transient simulation. Journal of Mechanics in Medicine and Biology. 2012; 12(01)
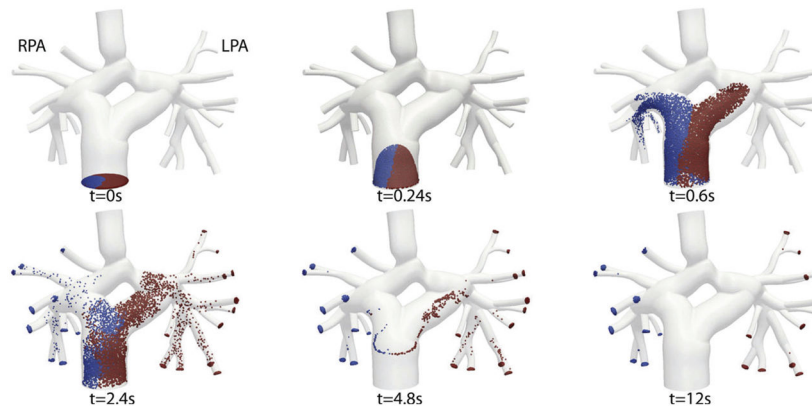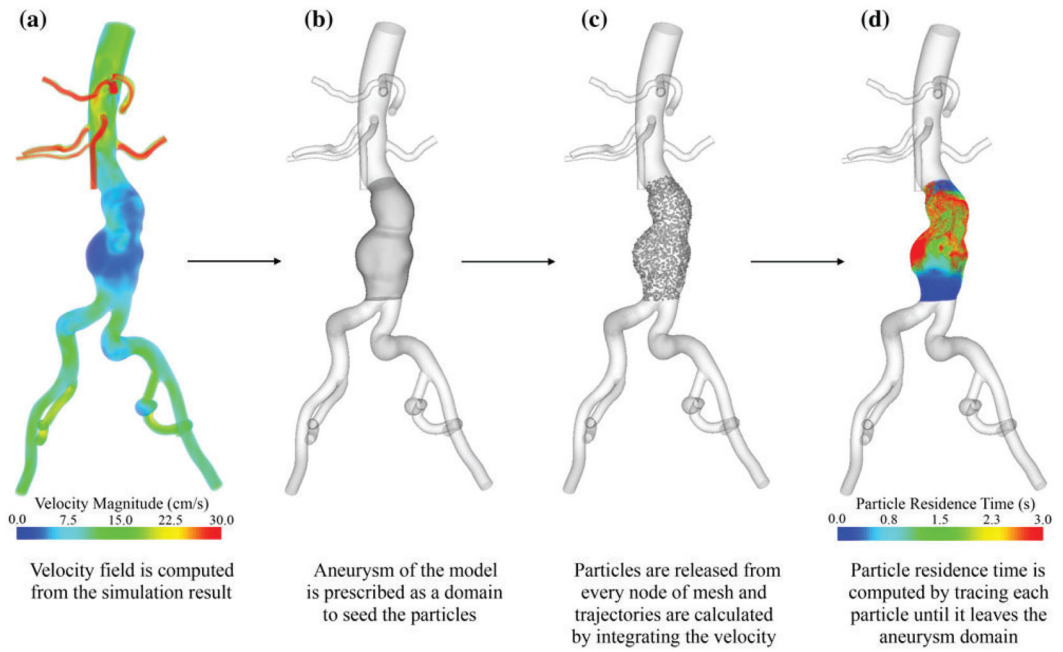
Figure 1.
Lagrangian particle tracking in a Y-graft model used to quantify inferior vena cava flow distribution to the left (LPA) and right (RPA) pulmonary arteries. Figure from Yang *et al.* [157] with permission.
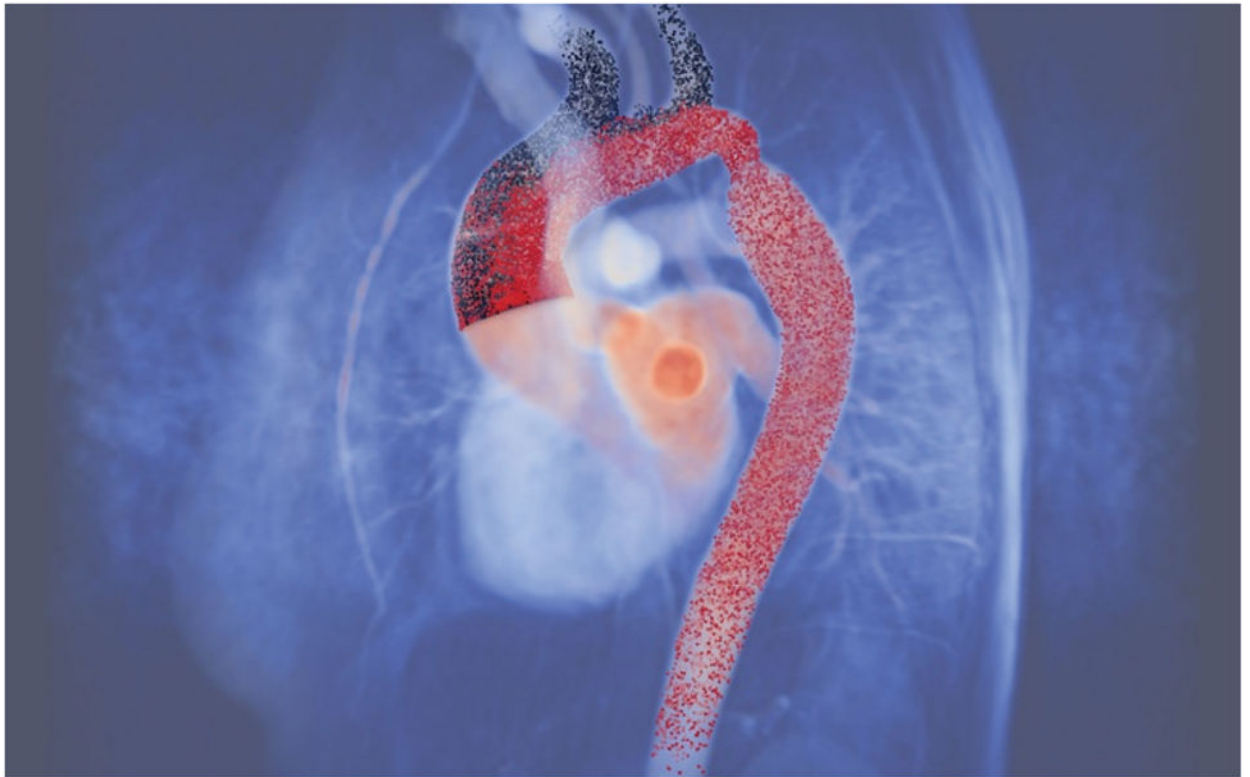
Figure 2.
Tracking inertial particles from the aortic valve through an aortic coarctation model. Particles are colored according to whether they are transported to the descending aorta or aortic arch branch arteries using methods described in [28].
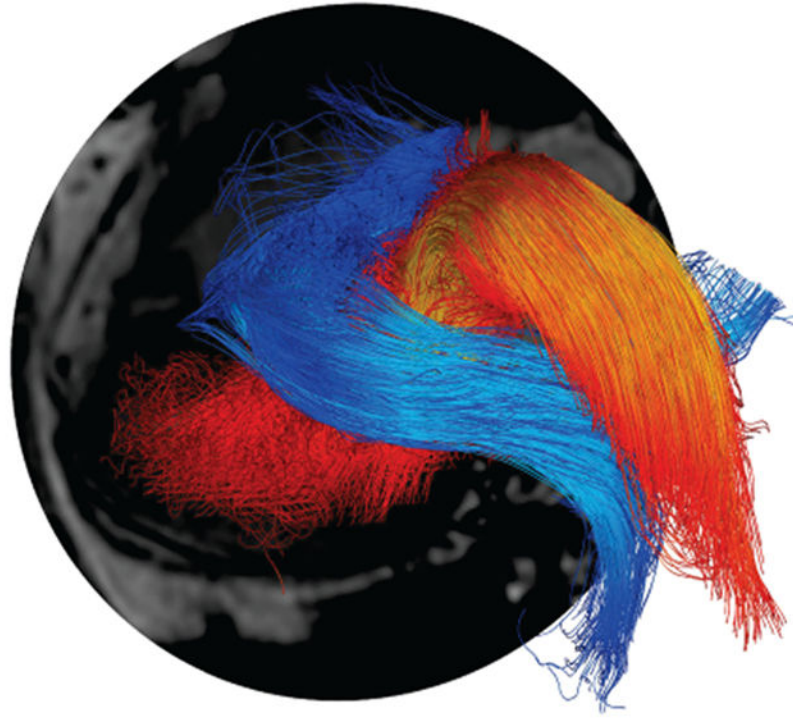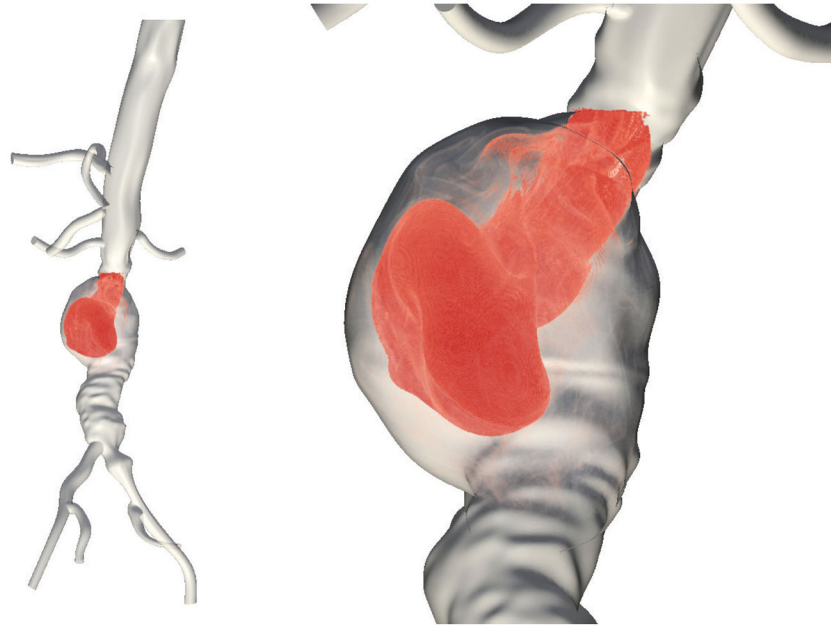
Figure 3.
Pathline visualization of systolic blood flow from the heart obtained by releasing tracers in the left and right ventricles during isovolumic contraction. The pathlines are computed from in vivo PCMRI velocity data by the methods described in Eriksson *et al.* [42]. Figure courtesy of Dr. Tino Ebbers.
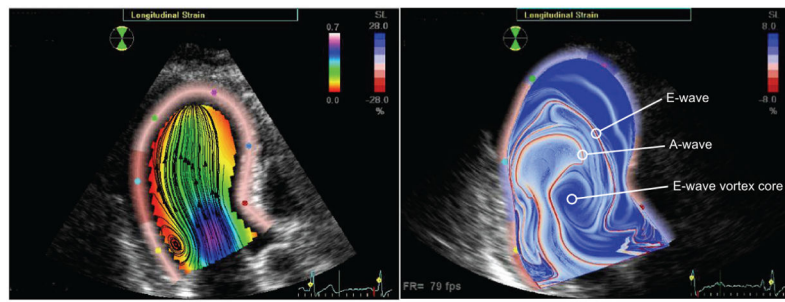
Figure 4.
The procedure used in computation of particle residence time (PRT). Tracers are released in a region of interest and integrated using the velocity data until they exit the prescribed domain. The time that each tracer takes to exit the domain is mapped to its initial location of release, resulting in the PRT field. Figure from Suh *et al.* [140] with permission.

Figure 5.
An attracting LCS delineates a large coherent vortex ring formed in an aortic aneurysm. This material surface defines the leading edge of the vortex [126, 128].

Figure 6.
Comparison of streamlines (left) and FTLE (right) from velocity field data reconstructed from Doppler echocardiography data at end of diastole. Distinct LCS revealed in the FTLE field denote the boundaries and evolution of E-wave and A-wave filling, along with respective vortex interaction.